Int. J. Electrochem. Sci., 14 **(2019)** 10729 – 10744, doi: 10.20964/2019.12.58

International Journal of ELECTROCHEMICAL SCIENCE
www.electrochemsci.org

Electrochemical, Optical and Impedance Studies on Photoactive Assemblies Consists of Mixed TiO_2-CdS Particles Occluded in Poly 2,2' Bithiophene in Aqueous Acetate Electrolytes

Sarah H. Osman, Antony Jeffers. Kasem K. Kasem[*]

School of Sciences, Indiana University Kokomo, Kokomo, IN, USA
[*]E-mail: kkasem@iuk.edu

Received: 5 June 2019 / *Accepted:* 27 September 2019 / *Published:* 29 October 2019

Amorphous nanoparticles of cadmium sulfide (CdS), titanium oxide (TiO_2), and 50/50 of TiO_2-CdS mixtures were prepared and immobilized in poly 2,2-bithiophene (PBTh) by occlusion electrodeposition method. X-ray studies indicated that a heterogeneous crystal structure of CdS (cubical-hexagonal) was formed. Optical studies indicated that occlusion of CdS or TiO_2 or both into PBTh significantly decreased the intensity of the inter band transition as revealed by the values of (E_d) dispersion energy. Photoelectrochemical (PEC) studies revealed evidence of fast charge recombination due to the hole accumulations at the interfaces. Furthermore, PEC studies indicated that, regardless of the method of the preparation of CdS-TiO_2 mixtures, CdS was the dominating factor in the photocurrent generation. . Electrochemical impedance spectroscopic studies (EIS) revealed that occluded assembly films possess a porous-type structure, with multiple phases as indicated by the generation of Nyquist plots with composite semi-circles. The study also shows that occlusion increased the frequencies of the dispersion and charge carrier hopping. The studied assemblies showed photostability for a long time of illumination. Photoelectrochemical, EIS, and optical outcomes did not follow monotonic properties of each component of these hybrid assemblies.

Keywords: CdS-TiO_2 mixtures, photoactive interfaces, optical, organic semiconductors, impedance

1. INTRODUCTION

Semiconductors (SC) with a large band gap have several advantages over those with a low band gap. Working at high temperature, performing in a harsh environment, stability, and possession of high switching frequencies are some of these advantages. However, the large band gap allows for absorption of only very narrow range of blue or UV energy, limiting its absorption activities. Overcoming this low absorption activity was the subject of many investigations. Sensitization of a large band gap with a small band gap SC was studied intensively. To name but few, small bandgaps of some Cd chalcogenides were

used to sensitize large bandgap TiO_2 that possesses a low-lying conduction band [1-5]. Some organic materials were also used to enhance the photoactivities of large band gap oxides. Dye-sensitized solar cells (DSSC) were first demonstrated in 1991[6] as example of sensitizing large band gap TiO_2 with some dyes. Several investigations [7-12] were performed with a goal of enhancing the photo conversion efficacy of DSSC. Common findings in these studies were that charge injection from one semiconductor into another can lead to efficient and longer charge separation. The dye or low band gap SCs can effectively capture the visible light and quickly transfer the photogenerated electrons into the TiO_2 conduction band.

Due to its diffuse nature of HOMO/LUMO, organic semiconductors are good candidates to couple with inorganic SC (native and/or modified) and widen the absorption range of solar radiation. This coupling will also achieve the construction of hybrid materials with an interface of large surface area. Success in sensitizing large bandgap inorganic SCs will lead to further development of hybrid functional materials. The sum of all properties of the hybrid materials is not a monotonic property outcome of individual components of the assembly, but it is an indication of strong synergy of sub-bands created within the hybrid interface [13-15]. Many applications have been reported for these hybrid materials in optics [16], electroactive materials [17] electrochromic materials [18] sensors [19], membranes [20] and biohybrid materials. [21, 22]. Further investigations were conducted in the field of creation of hybrid organic/organic [23-25] or organic /inorganic [26-27] interfaces. Characterization of the inorganic/organic/organic interface made of CdS/poly3-(2-thienyl) aniline (PThA)/poly 2,2 bithiophene (PBTh) was previously performed [28] . The photoactivities outcome was explained on basis of creation of hybrid sub-bands.

In this paper, we studied a hybrid assembly made of TiO_2-CdS occluded into PBTh. TiO_2 was sensitized by a low band gap CdS and further it was trapped into the low band gap photoactive organic polymer PBTh. The hybrid TiO_2-CdS/PBTh assembly was subject to optical, photo-electrochemical, and impedance studies to investigate if the properties outcome exhibit monotonic properties of each component of this hybrid assembly or not. This required comparison of the TiO_2-CdS/PBTh outcome with each of CdS/PBTh, and TiO_2/PBTh. Furthermore, we investigated the effects that the method of preparation may cause on the outcome of these assemblies.

2. EXPERIMENTAL

2.1. Reagents

The monomer 2,2- bithiophene (BTh), (Alfa Aesar) were used to prepare poly 2,2 bithiophene (PBTh). Other chemicals used in this study were of analytical grade. Deionized (DI) water was used to prepare aqueous electrolytes.

2.2 Preparations

TiO_2 nanoparticles were prepared as previously described [29]. TiO_2 sensitized with CdS (Codep. TiO_2/CdS) was prepared following a modified synthesis procedure previously published [30, 31]. CdS

was prepared as previously described [32]. A mechanical mixture of TiO_2 and CdS (Mec.TiO_2/CdS) was prepared as follows: 0.5 g of CdS nanoparticles were dispersed in Ti Iso-propoxide (in 80% ethanol) and stirred for 4 hours. The pale yellowish deposit was collected, washed and dried at 120 ^oC for 6 hours. The IOIs of each of TiO_2-CdS, CdS and TiO_2 occluded in PBTh were generated electrochemically using cyclic voltammetry (CV). This achieved through repetitive cycling of the FTO electrode potential between -0.5 and 1.7 V vs Ag/AgCl in an acetonitrile suspension (1 mg/mL) of the inorganic materials, 5 mM of the BTh monomer and 0.5 M $LiClO_4$.

2.3. Instrumentation

Electrochemical studies were performed in a 20 cm^3 three-electrode cell, consisting of a Pt flag as a counter electrode, a Ag/AgCl as reference electrode, and FTO with a surface area of 2.0 cm^2 as the working electrode. Photoelectrochemical studies of the thin solid films were performed using the experimental setup as described in previous work [28, 33]. A Solartron 2101A was used for the electrochemical impedance spectroscopy (EIS) studies. A BAS100W electrochemical analyzer (Bioanalytical Co. IN) was used to perform the electrochemical studies. Optical parameters were calculated based on the steady-state reflectance spectra, measured by a Shimadzu UV-2101PC spectrophotometer. An Olympus BX-FL Irradiation was performed with a solar simulator 300-watt xenon lamp (Newport, NJ) with an IR filter. All measurements were performed at 298 K.

3. RESULTS AND DISCUSSION

3.1 Structural Characterization

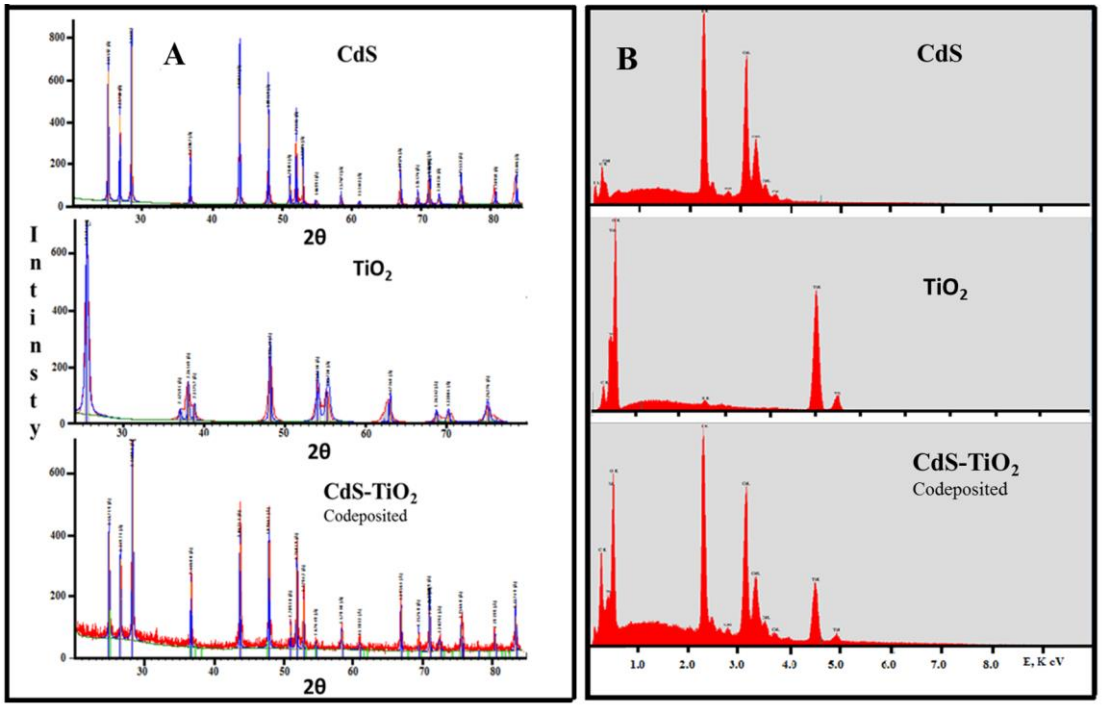

Figure 1. X-Ray studies of prepared samples, A) XRD patterns, B) XPS patterns.

Compounds CdS, TiO_2, and CdS-TiO_2 prepared as described in experimental section were subject to X-ray analysis. The results are displayed in Figure 1 A and B. It can be noticed the codeposition of CdS with TiO_2 generated a pattern that represents a mixture of both compounds. XRD analysis revealed that CdS showed hexagonal crystal structure, while the TiO_2 pattern indicates a tetragonal structure.

The pattern for the mixture of TiO_2-CdS, made by the codeposition method indicates that TiO_2 remained in the tetragonal crystal structure, while CdS gave a mixture of cubical and hexagonal crystal structures. On the other hand, a pattern of the CdS-TiO_2 mixture prepared by mechanical mixing of TiO_2 and CdS reveals only a hexagonal structure for CdS and tetragonal structure for TiO_2. This indicates that under the codeposition method conditions, a heterogeneous crystal structure of CdS (cubical-hexagonal) was formed.

3.2. Optical studies

Optical parameters such as α (absorption coefficient), n (refractive index), ε (dielectric constant), and σ_{opt} (optical conductivity) have been calculated and plotted as a function of photon energy. The results are displayed in Figures 2, 3 and 4.

3.2.1. Optical band gap studies

The absorption spectra of the assemblies TiO_2-CdS/PBTh, CdS/PBTh, and of TiO_2/PBTh are displayed in Figure 2, and indicate that occlusion of TiO_2 or CdS, or both, shifts the absorption peak to photon energies greater than that of the host polymer PBTh. Furthermore, the number of photons absorbed by the TiO_2-CdS/PBTh, CdS/PBTh, and TiO_2/PBTh is greater than that absorbed by PBTh as evident by area under the peak in Figure 2. The treatment of the absorption data for all studied assemblies were listed as described in previous study [34]. The data listed in Table 1, were generated from the resultant plots of $\alpha^{1/2}$ vs photon energy (hυ) and $(\alpha * h\upsilon)^2$ vs hυ, respectively. The quantities listed in Table 1 indicate that the absorption behavior of the host film was dominating the assembly's behavior. Both the host polymer, PBTh, and the assembly showed direct and indirect band gaps. This may be attributed to fact that the diffusive highest occupied molecular orbitals (HOMO) and lowest unoccupied molecular orbitals (LUMO) for PBTh bridged the energy levels (VB, CB, E fermi) for the occluded CdS, TiO_2 or the mixtures of both. This is because the occlusion of TiO_2 modified with PBTh, created hybrid sub-bands with a smaller band gap between the highest occupied molecular orbitals (HOMO) and lowest unoccupied molecular orbitals (LUMO) of the host polymer. Table 1 also indicates that the occlusion of CdS and or TiO_2 reduces absorption band tails attributed to energy band tail or Urbach energy [35] in the host polymer PBTh. The Urbach energy values listed for the IOI CdS/PBTh assemblies still greater than that recoded for thin films of CdS [36], while that of TiO_2/PBTh is much smaller than that reported for TiO_2 thin films [37] at room temperature. Furthermore, the Urbach energy listed for the TiO_2-CdS/PBTh (codeposition) is smaller than that of pure TiO_2 thin film and greater than that of pure CdS.

It is important to mention that the methods of preparations of the referenced assemblies are totally different from the occlusion method used in this study.

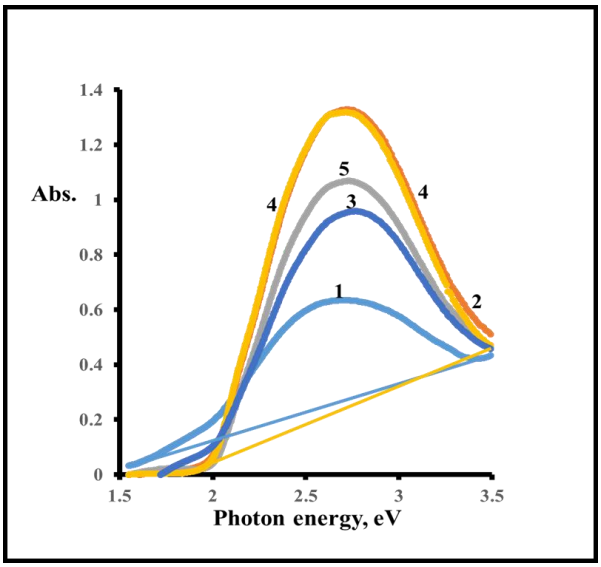

Figure 2. Absorption spectra of 1-PBTh, 2- PBTH/TiO_2, 3- PBTh/CdS, 4- PBTh/CdS-TiO_2 (mech.), and 5- PBTh/Cds-TiO_2 (codeposition).

Table 1. Optical band gap for the studied assemblies.

Assembly	≈ band gap at λ max, eV	Direct band gap, eV	Indirect band gap, eV	Urbach energy, eV
PBTh	2.4	2.0	1.1	0.76
PBTh/TiO_2-CdS (Mech)	2.8	2.2	1.9	0.07
PBTh/TiO_2-CdS (Codepos.)	2.8	2.25	1.9	0.125
PBTh/CdS	2.6	2.2	1.9	0.07
PBTh/TiO_2	2.8	2.2	1.9	0.08

3.2.2. Optical parameters

3.2.2.1 Refractive index, n

The plot of refractive index (n) vs wavelength is displayed in Figure 3. While PBTh did not exhibit a large increase in n over all the studied wavelengths, the values of n for PBTH/TiO_2, PBTh/CdS, PBTh/CdS-TiO_2 (mech.) and PBTh /Cds-TiO_2 (codeposition) show a sharp increase at wavelengths shorter than 620 nm (2 eV) and reached maximum values at a photon energy around 2.5 eV. No tangible change was observed at photon energies greater than 2.5 eV.

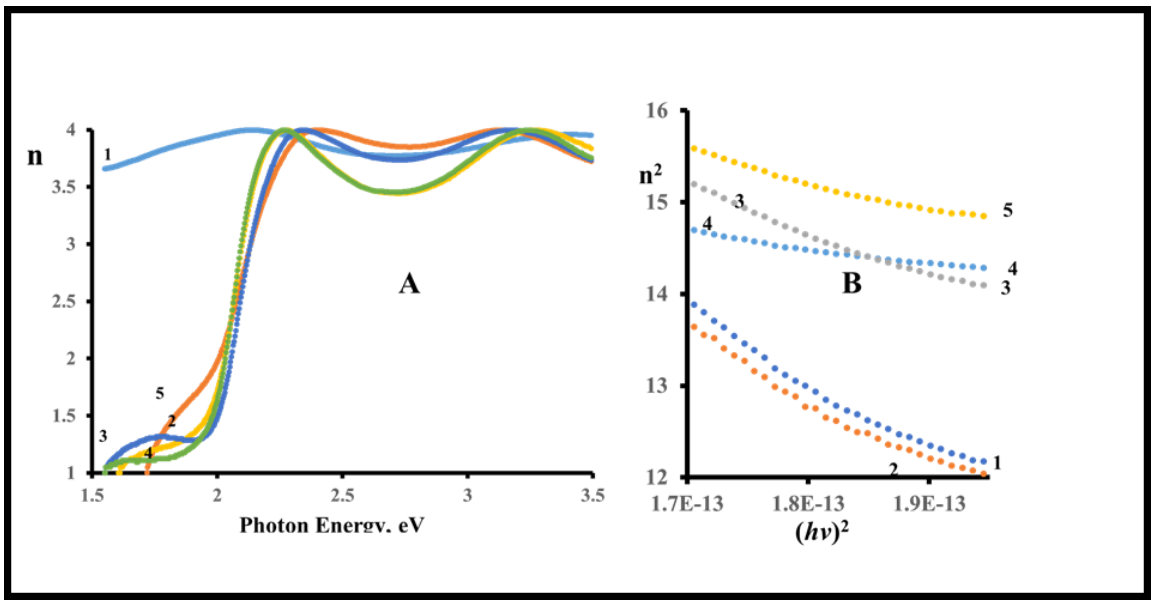

Figure 3. Refractive index vs photon energy **A)** n vs *hv*, **B)** n^2 vs $(hv)^2$, 1-PBTh 2- PBTH/TiO_2 3- PBTh/CdS, 4- PBTh/CdS-TiO_2 (mech.) 5- PBTh/Cds-TiO_2 (codeposition)

Dependence of the complex refractive component on the wavelength can be linked to the optical properties of solid materials. The following equation [38] describe such dependence

$$[n^2(h\nu) - 1]^{-1} = -(E_o E_d)^{-1}(h\nu)^2 + {}^{E_o}/_{E_d} \qquad 1$$

The plot of $[n^2(h\nu) - 1]^{-1}$ vs $(h\nu)^2$ should give a slope = $(E_oE_d)^{-1}$ and intercept =E_o/E_d. where E_o and E_d refer to oscillator energy, and dispersion energy respectively. Furthermore the relation of the refractive index to the lattice dielectric constant ε_L can be seen in the following equation [39]:

$$n^2 = \varepsilon_L - \left[\frac{e^2}{\Pi C^2}\right]\left[\frac{N}{m^*}\right]\lambda^2 \qquad 2$$

Figure 3B indicates that the plot of n^2 vs λ^2 generates a straight line with intercept equal ε_L.E_o, E_d and ε_L for all studied assemblies are listed in Table 2

Table 2. Some optical parameters for the studied assemblies.

Assembly	E_d, eV	E_o, eV	Lattice Dielectric constant $\boldsymbol{\varepsilon_L}$	Optical band gap, eV
PBTh	8.20	2.14	15.093	2.4
PBTh/CdS	1.73	2.54	24.715	2.8
PBTh/TiO_2	0.84	2.18	29.07	2.8
PBTh/CdS-TiO_2 (Codepsited)	1.88	2.13	20.975	2.6
PBTh/CdS-TiO_2 (mechanical mix.)	0.82	2.26	28.507	2.8

The data in Table 2 clearly show that E_d, as a measure of the intensity of inter-band optical transition, is independent of a band gap. Occlusion of CdS or TiO_2 or both into PBTh significantly decreased the intensity of inter-band transition. No tangible change in the values of E_o was observed. Furthermore, the value of ε_L in Table 2 , listed for mechanical mix of TiO_2 and CdS is closer to that of PBTh/TiO_2 which indicates that TiO_2 was a greater contributor than CdS in this mixture. When PBTh polymer serves as the matrix polymer, the CdS and TiO_2 or their mixtures serve inorganic fillers to increase the effective dielectric constant, the studied assemblies can be potential materials for energy storage.

3.2.2.2 Dielectric constants

The plot of the ε_r (real component of dielectric constant) vs photon energy in Figure 4 clearly shows a sudden rise in the ε_r at photon energy around 2.1 eV and mild decrease in ε_r values around 2.7 eV. Further, the values of ε_r for PBTh/TiO_2 were very close to those of PBTh/TiO_2-CdS (mechanical mixture), which indicate that the TiO_2 component in the mixture was the dominant factor. The variation of ε_r around the 2.1-2.9 eV of photon energy range indicates that the photon/electron interaction took place within this range. The polarizability of materials generates their dielectric properties at a given frequency [40]. Electron exchange between Cd or Ti atoms in CdS or TiO_2 respectively, and S atoms of PBTh, can cause local displacement of electrons and induces interfacial polarization. Figure 4 shows that CdS-TiO_2 has some effect on PBTh polarizability within photon energy range between 2.4 and 3.1 eV.

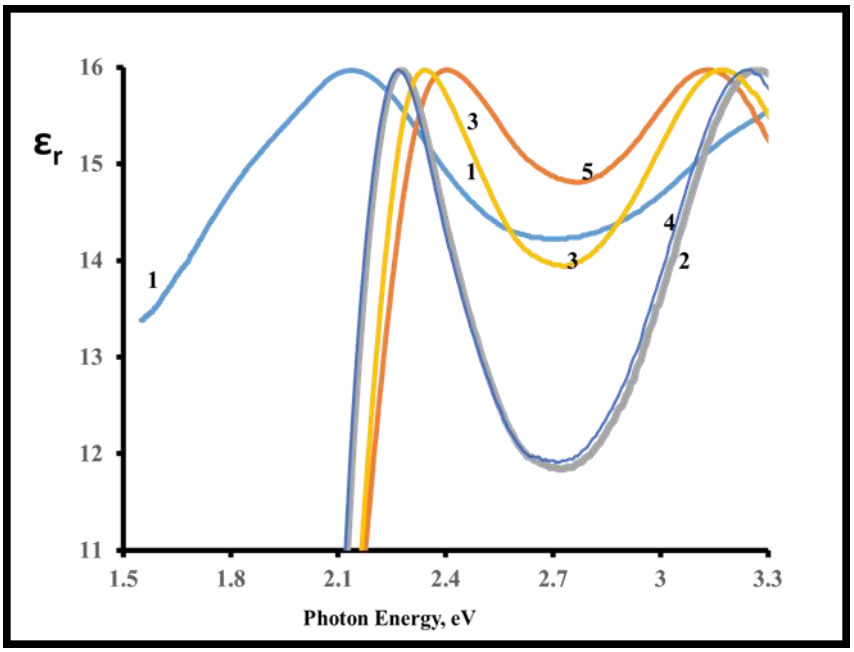

Figure 4. Real ε_r, components of dielectric constant for 1-PBTh, 2-PBTH/TiO_2, 3-PBTh/CdS, 4-PBTh/CdS-TiO_2 (mech.), and 5- PBTh/Cds-TiO_2 (codeposition)

3.2.2.3 Optical conductivity σ_{opt} and Electrical conductivity σ_{ele}

Both $\boldsymbol{\sigma_{opt}}$ and $\boldsymbol{\sigma_{ele.}}$ were calculated using the following formulas [41-42]:

$$\sigma_{opt} = \frac{\alpha nc}{4\Pi} \quad (3)$$

and

$$\sigma_{ele} = \frac{2\lambda\, \sigma_{opt}}{\alpha} \quad (4)$$

Figure **5** clearly shows that 1) σ_{opt} increases with increasing photon energy up to 2.9 eV after which starts to decrease, 2) both PBTH/TiO_2 and PBTh/CdS-TiO_2 (mech.) has a greater conductivity than all studied assemblies, 3) the fact that $\boldsymbol{\sigma_{opt}}$ of PBTh/TiO_2 is equal to that of PBTh/CdS-TiO_2 (mech.) indicates that TiO_2 is the dominant factor in the mechanical mixture with CdS. And 4) the sharp rise around the band gap of each assembly can be attributed to the electron excitation at range of photon energy. At a photon energy greater than 3 eV, the optical conductivity decreases. Such behavior can be attributed to the dopant‘s inability to provide the host polymer with an additional charge transfer [38]. Figure 5B indicates that optical conductivity is much greater than electrical conductivity. Such behavior can be explained on the basis of the Drude model [43].

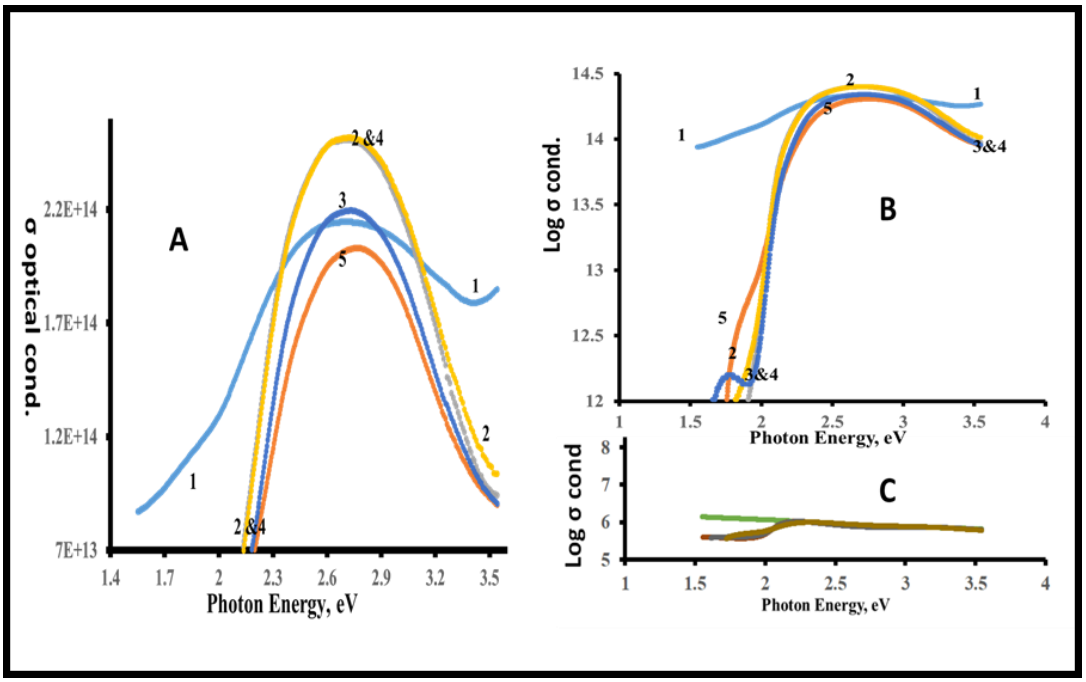

Figure 5. Conductivity (optical $\boldsymbol{\sigma_{opt.}}$& electrical $\boldsymbol{\sigma_{ele}}$) vs photon energy plots of **A)** $\boldsymbol{\sigma_{opt}}$ and **B)** Log of $\boldsymbol{\sigma_{opt}}$ and log $\boldsymbol{\sigma_{ele.}}$ vs photon energy for 1-PBTh, 2- PBTH/TiO_2, 3- PBTh/CdS, 4- PBTh/CdS-TiO_2 (mech.), and 5- PBTh/Cds-TiO_2 (codeposition), C) log $\boldsymbol{\sigma_{ele.}}$ vs photon energy

In the absence of alternating frequency, optical conductivity can be considered as electrical conductivity.

3.3. Photoelectrochemical behavior

The electrochemical studies on FTO/PBTh occluded with TiO_2, with CdS, and with CdS-TiO_2 were achieved by cycling the potential of FTO modified with each these assembly in acetate electrolyte (pH 7.6). The studies were performed in dark and under illumination, with scan rate 0.10V/s, between, unless otherwise stated, -1.0 to 1.0 V vs Ag/AgCl. The results are displayed in Figures 6,7, 8, 9 and 10.

3.3.1 Electrochemical behavior of FTO/PBTh in Acetate electrolyte

The results displayed in Figure 6 show that a great photocurrent was produced in the cathodic scan in a range between ≈0.3 V -1.1 V. In the anodic scan, the current under illumination (photocurrent) exceeded the current reported in dark (dark current) at 0.2 V vs Ag/AgCl. This indicated the approximate position of E_{fb} (flat band potential). This corresponds to 5.0 eV vs vacuum scale.

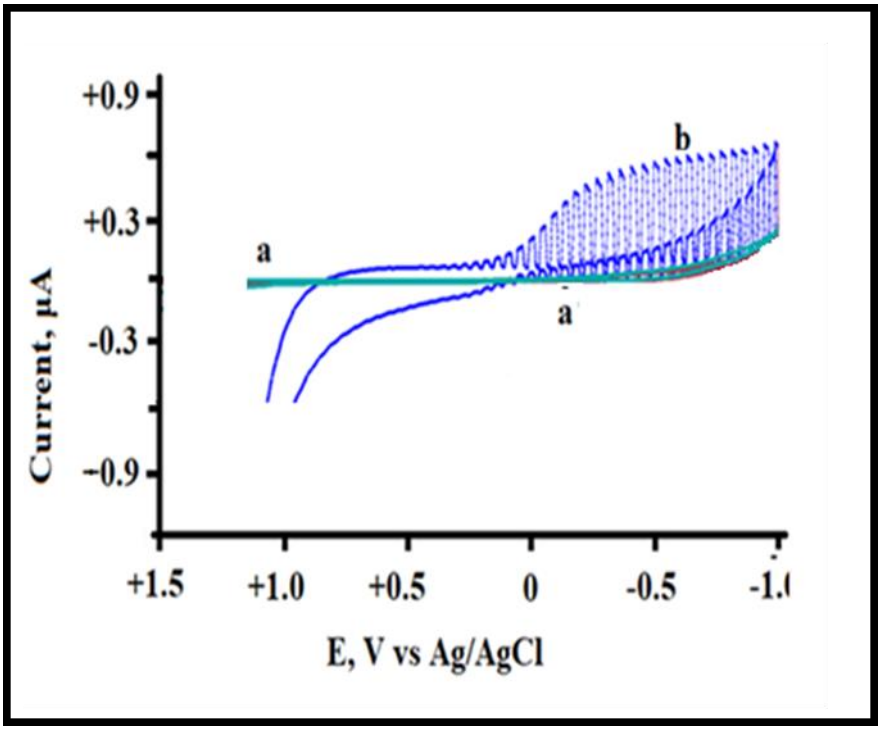

Figure 6. CV of FTO /PBTh in 0.2 M acetate electrolyte (pH 8) at 0.10V/s: a) dark, and b) under illumination

3.3.2 Electrochemical behavior of FTO/CdS/PBTh in acetate electrolyte

Figure 7 displays the CV behavior of this assembly in an acetate electrolyte. The magnitude of the generated photocurrent was less than that generated from FTO/PBTh (Figure 6). However, there is no tangible changes in the potential where the photocurrent exceeded the dark current, as shown in Figure

7. The photocurrent generated in this assembly is greater than that reported for CdS modified by poly 3-(2-thienyl) aniline and occluded in PBTh [28].

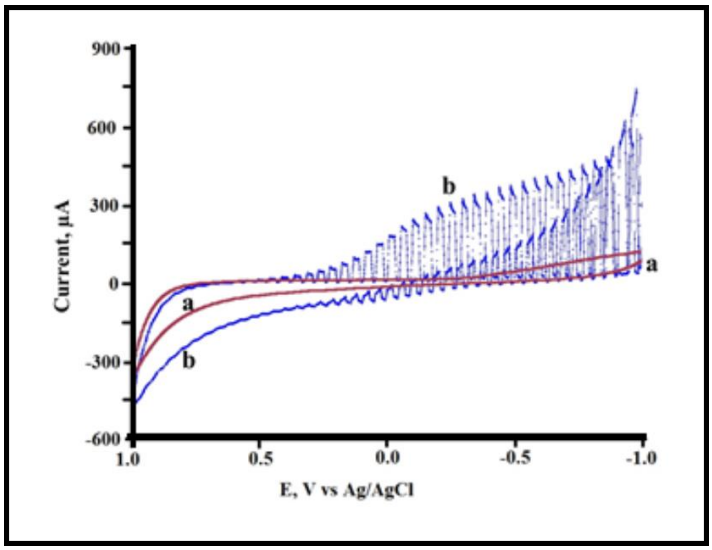

Figure 7. CV of FTO/CdS/PBTh in 0.2 acetate electrolyte a) dark, and b) under illumination

3.3.3 Electrochemical behavior of FTO/TiO_2/PBTh in Acetate electrolyte

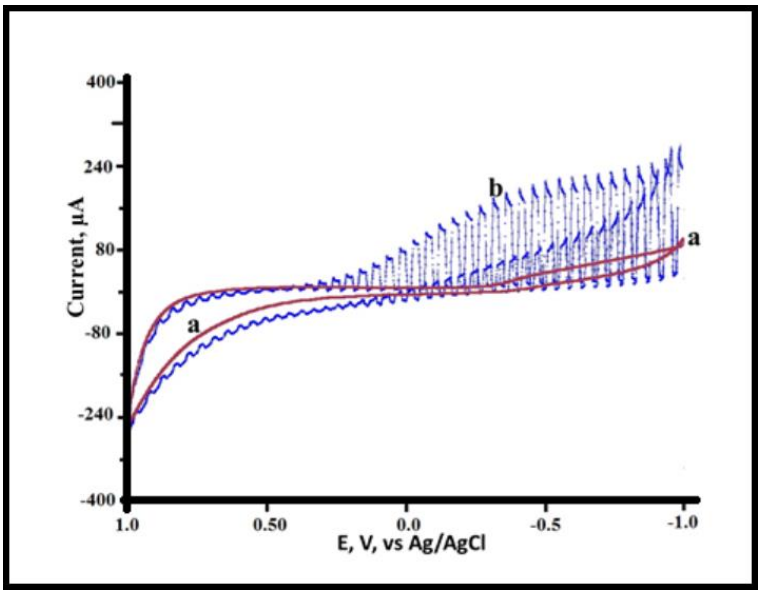

Figure 8. CV of FTO/ TiO_2/PBTh in 0.2 acetate electrolyte a) dark, and b) under illumination.

The electrochemical behavior of the FTO/TiO_2/PBTh assembly in acetate electrolyte is displayed in Figure 8. The photo current generated by this assembly is less than that recorded for the PBTh (Figure 6) and less than that of CdS/PBTh (Figure 7). The photocurrent generated in this assembly is greater than that reported for TiO_2 modified by poly 3-(2-thienyl) aniline and occluded in PBTh [44]. However, no tangible changes in the E_{fb} potential occurred. The low photocurrent can be attributed to a greater

band gap of TiO_2/PBTh than those of PBTh or CdS/PBTh. This greater band gap allows for only photons with corresponding energy to be absorbed.

3.3.4 Electrochemical behavior of FTO/CdS-TiO_2/PBTh in acetate electrolyte

Figures 9 and 10 display the CV behavior of FTO/ CdS-TiO_2 (mech.)/PBTh, and that of FTO/CdS TiO_2 (codeposition)/PBTh in acetate electrolyte, respectively. The photocurrent generated in the cathodic scan is greater than those generated for all other assemblies. This was also observed in Figure 11. This indicate indicates that both CdS/TiO2 mixture occluded in PBTh contributed to such increase regardless of preparation method. The greater number of photons absorbed by the FTO/CdS-TiO_2 (mech.)/PBTh, and by FTO/CdS-TiO_2 (codeposition)/PBTh as indicated from Figure 2 may cause this increase in the photocurrent.

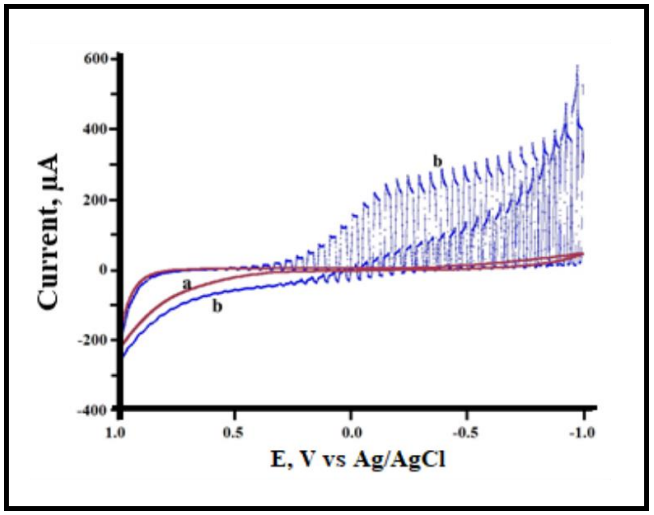

Figure 9. CV of FTO/ CdS-TiO_2 (mech.)/PBTh in 0.2 acetate electrolyte; a) dark, and b) under illumination.

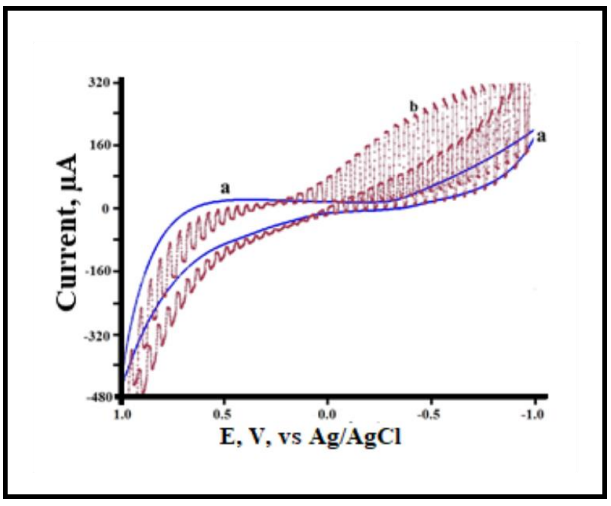

Figure 10. CV of FTO/ CdS-TiO_2 (Codeposition)/PBTh in 0.2 acetate electrolyte a) dark, and b) under illumination.

Figure 11A shows the photocurrent-time plot for all studied assemblies. It is worth notice that illumination of any of the occluded assemblies causes a sharp anodic current spike. Such behavior was reproducible. This is evidence of the fast charge recombination due to the hole accumulations [45] at the outermost layers of the assembly electrolyte interface. Such behavior was not observed for FTO/PBTh in an acetate electrolyte (Figure10B). Furthermore, in the dark, no backflow of electrons from the substrate FTO to the assembly body took place as is evident from the lack of cathodic current (reversed transient current).

Figures 11A and B also show that PBTh occluded and non-occluded showed photostability as the magnitude of the recorded photocurrent in each trial were similar.

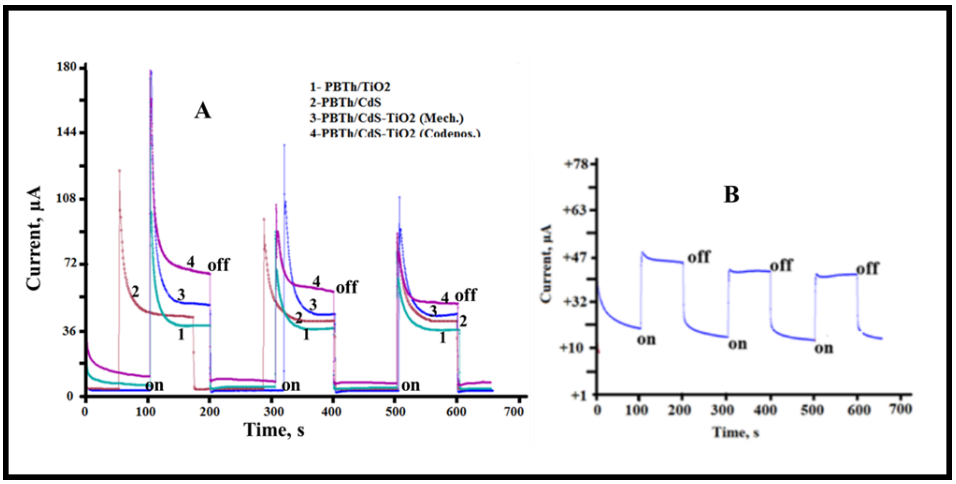

Figure 11. Photocurrent-Time plot at -0.5 V vs Ag/AgCl in acetate electrolyte for A) 1-FTO/PBTh/TiO_2, 2- FTO/PBTh/CdS, 3- FTO/PBTh/TiO_2-CdS (Mech.), and 4-FTO/PBTh/TiO_2-CdS (Codeposit.). B) For FTO/ PBTh only, on = illumination, off = dark

3.4. Electrochemical impedance spectroscopic studies

Impedance spectra of the studied assemblies were measured and analyzed between 10^5 -10^{-2} Hz in a three-electrode cell containing acetate electrolytes. Figure 12 display Nyquist plot obtained for FTO/PBTh-CdS and that of FTO/PBTh. Figure 12Aa shows. Both kinetic control at high frequency and diffusional control at low frequency were observed for FTO/PBTh only (Figure 12Aa). The shape of un-concentered semicircle at high frequencies (Figure 12Ab) is indication of the film porosity [46]. While the Nyquist plots generated for other assemblies are not displayed, the EIS data such as W_m (Binding energy), s (temperature dependent parameter), relaxation frequency and τ(s) (Relaxation time) for all studied assemblies are listed in Table 3. Illuminated FTO/CdS/PBTh (Figure12Ab) shows composite shape semicircles. Such shapes show: 1- if the charge transfers in one or both semicircles are very fast, and/or 2-if the time constants for exchange reactions are similar. It is possible that the heterogeneity of inorganic (CdS)/organic (PBTh) interface, and the closer value of the band gap of CdS to that of PBTh lead to creation of two phases. Upon illumination, these two phases responded with same time constant. Neither FTO/PBTh nor FTO/CdS/PBTh (in the dark) generated Nyquist plots with composite shapes (Figure 12Aa and 12Ac). Generation of composite shape semicircles was observed

with FTO/CdS-TiO_2 /PBTh assemblies but was not observed with the FTO/TiO_2/PBTh assembly. This will lead us to believe that the presence of CdS contributed in generation of these composite shape semicircles.

AC conductivity σ_{ac}.

The σ_{ac} was calculated using the following equation [47].

$$\sigma_{ac} = \frac{L}{A} * \frac{Z\prime}{Z\prime^2 + Z"^2} \quad (5)$$

According to the following equation [48]:

$$\sigma_{ac} = \sigma_{dc} + A\omega^S \quad (6)$$

where A is the strength of polarizability**,** s is temperature-dependent parameter which can be determined from the slope of line of the plot of log $\boldsymbol{\sigma_{ac}}$ vs log ω.

$$\log \sigma_{ac} = \log \sigma_{dc} + \log A + S \log \omega \quad (7)$$

The plot of log σ_{ac} vs log ω is displayed in Figure 12C. This figure shows that in this low frequency region, the conductivity is almost independent of frequency, while at high frequencies, the conductivity increases. This can be attributed to increased dispersion and charge carrier hopping [47]. The crossing of the positively sloped line with the base line at high frequencies represents the hopping frequency. Figure 12C shows that occlusion of PBTh with CdS caused increasing in the hopping frequency.

The energy required to remove one electron from one site to another within the film structure (W_m) or binding energy, can be calculated from the following relation [49]:

$$W_m = \frac{6k_BT}{1-s} \quad (8)$$

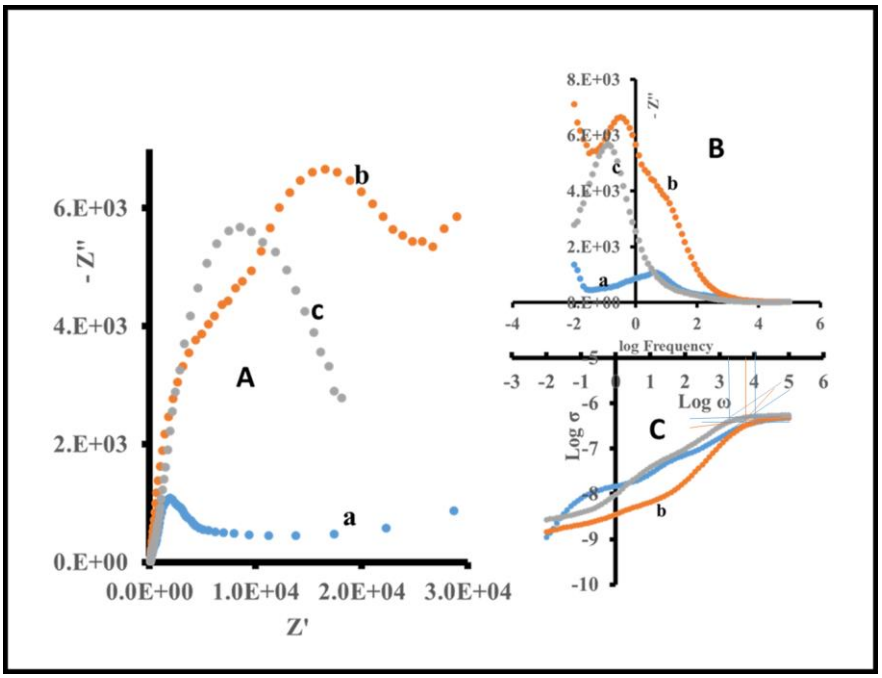

Figure 12. A) Nyquist plot in 0.2 M acetate electrolytes (pH 6) at -0.5V vs Ag/AgCl **,** B) Bode's plot for a- FTO/PBTh-CdS (In dark), b) FTO/PBTh-CdS (illumination), and c) FTO/ PBTh , and C) log σ (Conductivity) vs log frequency.

Table 3 shows that occlusion of CdS, TiO_2, or CdS-TiO_2 in PBTh increases the W_m, and decreases the relaxation time calculated from log ω at maximums in figure 12B. W_m is inversely proportional to the charge carrier hopping distance [47]. The greater the W_m, the smaller the hopping distance. The data listed in Table 3 indicate that occlusion of CdS, TiO_2 or both in PBTh increased the W_m, consequently decreasing the carrier hopping distances.

Table 3. Electrochemical impedance data for the studied assemblies

Property	PBTh	PBTh-CdS		PBTh-TiO_2		PBTh-TiO_2/CdS (codeposition)		PBTh-TiO_2/CdS (mechanical)	
		D	L	D	L	D	L	D	L
S	0.495	0.432	0.765	0.825	0.949	0.750	0.776	0.799	0.641
W_m(eV)	0.301	0.268	0.648	0.880	3.02	0.688	0.616	0.766	0.429
ω (Hz)	0.126	3.981				1.0		4.986	
τ(s)	1.26	0.04				0.159		0.200	

4. CONCLUSION

The occlusion of CdS, TiO_2, and mixtures of CdS-TiO_2 in PBTh, allowed absorption of broad wavelengths in the blue zone which makes both materials and their I/O/O/I assemblies potentially useful in solar energy harvesting systems. Photoelectrochemical and EIS, and optical outcome did not follow monotonic properties of each component of these hybrid assemblies. No tangible changes were observed because of the method of preparation of CdS-TiO_2 mixtures.

ACKNOWLEDGEMENT
The authors acknowledge Office of the Academic Affairs at Indiana University Kokomo for supporting this project.

References

1. F. Ke, H. Jinzhao, Y. Nannan, X. Xijin, W. Mingzhi, *Indust & Engin. Chem. Research*, 54(2) (2015)659.
2. Z. Chen and Y.-J. Xu, *ACS Appl. Mater. Interfaces*, *5* (24) (2013)13353. DOI: 10.1021/am4043068
3. T. C. Dang, D. L. Pham, H.C Le and V. H. Pham, *Adv. Nat. Sci.:Nanosci. Nanotechnology*. 1 (2010) 015002. doi:10.1088/2043-6254/1/1/015002.
4. M.E. Hernández-Torres, M. T. Ojeda-Carrera, M. Sánchez-Cantú, N. R. Silva-González, and J. M. Gracia-Jiménez*, Chemical Papers,* 68 (9) (2014)1257.
5. S. Biswas, M. F. Hossain, T. Takahashi, Y. Kubota, A. Fujishima, *Phys. Stat. Solidi A: Appl. Mater. Science,* 205(8) (2008) 2028.
6. B. O'Regan,and M.Gratzel. *Nature,* 53(1991)737.
7. S. Mathew, A. Yella, P. Gao, *Nat. Chemistry,* 6(2014) 242.

8. M. A. A. Sadatlu and N. Mozaffari, *Solar Energy,* 133 (2016) 24.
9. D. Sengupta, P. Das, B. Mondal, and K. Mukherjee. *Renew. Sust. Ener. Reviews*, 60 (2016) 356.
10. P. Tiwana, P. Docampo, M.B.Johnston, H. J. Snaith, and L.M. Herz, *ACS Nano*, 5(6)(2011) 5158.
11. D. Sengupta, P. Das, U. Kasinadhuni, B. Mondal, and K. Mukherjee, *J .Renew. Sust. Energy*, 6(6) (2014). ID063114,
12. D. Barpuzary, A. Banik, A. N. Panda, and M. Qureshi, *J. Phys. Chemistry* C, 119 (2015)3892.
13. C. Sanchez, G. J. A. Soler-Illia, F. Ribot, D. Grosso, *Chimie*, 6(2003)1131.
14. C. Sanchez, G.J.A.A. Soler-Illia, F. Ribot, T. Lalot, C. R. Mayer, V. Cabuil, *Chem. Mater.*, 13(2001)3061.
15. S. H. Mir, L. A. Nagahara, T. Thundat, P. Mokarian-Tabari, H. Furukawa, and A. Khosla, *J. Electrochem. Society*, 165(8)(2018) B3137.
16. J.H. Harreld, B. Dunn, J.I. Zink. *J. Mater. Chem*istry, 7(1997)1511.
17. Y. Guo, A. Mylonakis, Z. Zhang, G. Yang, P. I. Lelkes, S. Che, Q. Lu, and Y. Wei, *Chem. A Eur. J.*, 14 (2008)2909.
18. J. Fei, K. G. Lim, and G.T. R. Palmore, *Chem. Material*, 20(2008)3832.
19. Z. Fang, S. Wang, L. Zhao, B. Dong, Z. Xu, J. Ren, and Q. Yang, *Mater. Letters*, 62(2008)1514.
20. S. E. Nam, S. O. Kim, Y. Kang, J. W. Lee, and K. H. Lee*, J. Membr. Sci*., 322(2008)466.
21. E. Landi, S. Martorana, A. Tampieri, S. Guicciardi, and C. Melandri, *Key Eng. Mater*., 361(2008) 547.
22. M. Darder, P. Aranda, and E. Ruiz-Hitzky, *Adv. Mater*., 19(2007)1309.
23. W. Osikowicz, M.P. de Jong, W.R. Salaneck, *Adv. Mater*, 19(2007)4213
24. A. Wan, J. Hwang, F. Amy, A. Kahn. *Org. Electron*., 6(2005)47.
25. S. Braun, R. W. Salaneck, and M. Fahlman. *Adv. Mater*. 21(2001)450.
26. S. Ananthakumar, J. Ramkumar, S. M. Babu, *Mat. Sci. Semicond. Processing,* 22 (2014)44.
27. M. Otero , T. Dittrich , J. Rappich , D.A. Heredia , F. Fungo, E. Durantini , L.Otero, *Electrochim. Acta*, 173(10) (2015)316.
28. K. K. Kasem, H. Worley and M. Elmasry. *Advn. Compos. Hybr. Mater.,*1(2018) 748. https://doi.org/10.1007/s42114-018-0055-0
29. H.Y. Lee and G. M. Kale, *Int. J. Appl. Ceram. Technology*, 5(6)(2008),657. DOI:10.1111/j.1744-7402.2008.02248.x
30. B. Huang, Y. Yang, X. Chen, D. Ye, *Catal. Communications,*11(2010) 844.
31. M. Wu, G. Lin, D. Chen, G. Wang, D. He, S. Feng, and R. Xu, *Chem. Mater.*, 14(2002)1974.
32. Z. R. Khan M. Zulfequar, M.S. Khan, *J. Mater. Science,* 46(2011)5412.
33. K.K Kasem, M. Elmasry, K. Baker, and C. Santucci, *Thin Solid Films*, 634 (2017)56.
34. J. Tauc, *Mater. Res. Bulletin*, 3(1968)37.
35. F. Urbach., *Phys. Review*, 92 (1953)1324.
36. S. J. Ikhmayies, and R. N.Ahmad-Bitar, *J. Mat. Res. Technology,* 2(3) (2013)221.
37. F. Hanini, A. Bouabellou, Y. Bouachiba, F. Kermiche, A. Taabouche, M. Hemissi, and D. Lakhdari, *IOSR J. Engineering,* 3(11) (2013)21.
38. S. H.Wemple, M.D. DiDomenico, *Phys. Review* B, 3(1970)1338.
39. G.A. Kumar, J. Thomas, N. George, B.A. Kumar, P.R. Shnan, V.P. Npoori, and N.V. Unnikishnan, *J. Phys. Chem. Glasses*, 41(2001)89.
40. M.T. Ramesan. *J. Thermoplast. Compos. Mater.,* 28(2015)1286.
41. P. Sharma, and S.C. Katyal, *J. Physics D: Appl. Physics*, 40(7)(2007)2115. https://doi.org/10.1088/0022-3727/40/7/038.
42. G. Sabari, and T.C. Dhanushkodi. *Cryst. Res. Tech*., 44(12)(2009)1297. https://doi.org/10.1002/crat.200900351.
43. P. Drude, *Zur Elektronentheorie der Metalle. Annalen der Physik,* 306 (3)(1900)566.
44. K. K. Kasem, H. Sadou, H. Worley, and J. Wegner, *J. Mat. Sci. Chem. Engineering,* 6(2018) 50.

45. M. Sookhakian, Y.M.Amin, S. Baradaran, M.T. Tajabadi, A. M. Golsheikh, and W.J. Basirun, *Thin Solid Films*, 552(2014)204.
46. H. Kaiser, K.D. Beccu, M.A. Gutjahr. *Electrochim. Acta,* 21(1976)539.
47. J.H. Joshia, D.K. Kanchan, M.J. Joshi, H.O. Jethva, K.D. *Mat. Res. Bulletin,* 93(2017)63.
48. A.K. Jonscher. A.K. *Nature*, 267(1997), 673, 10.1038/26763a0.
49. K. Funke. *Prog. Sol. State Chemistry*, 22(1993)111.